IEEE Access
Multidisciplinary | Rapid Review | Open Access Journal

Received August 28, 2019, accepted September 5, 2019, date of publication September 10, 2019,
date of current version September 25, 2019.

Digital Object Identifier 10.1109/ACCESS.2019.2940635

A Single-Layer SIW Slots Array Monopulse Antenna Excited by a Dual-Mode Resonator

TIANMING YANG[1], ZHIQIN ZHAO[1], (Senior Member, IEEE), DEQIANG YANG[1], XIANFENG LIU[1], AND QING-HUO LIU[2], (Fellow, IEEE)

[1]School of Electronic Science and Engineering, University of Electronic Science and Technology of China, Chengdu 611731, China
[2]Department of Electrical and Computer Engineering, Duke University, Durham, NC 27708, USA

Corresponding author: Deqiang Yang (dqyang@uestc.edu.cn)

This work was supported in part by the National Natural Science Foundation of China under Grant 61721001 and Grant 61871083, and in part by the Sichuan Science and Technology Program under Grant 2018GZ0230.

ABSTRACT The conventional monopulse comparator, which commonly consists of a power divider, a standard 3dB-coupler and a 90-degree phase shifter, occupies a significantly large area of the antenna aperture. This results in a low efficiency. In order to improve the antenna's aperture efficiency and keep a planar single-layer structure simultaneously, a substrate integrated waveguide (SIW) slots array monopulse antenna excited only by a square dual-mode (TE_{120} and TE_{210}) SIW resonator is proposed, fabricated and measured in this communication. The sum and difference beams are obtained when the feeding cavity operates at two high-order modes, respectively. The needless of complex feeding network reduces the antenna's structure complexity and improves its aperture efficiency. The aperture efficiency of the antenna can reach 42%. Besides, the sum and difference ports have good isolation due to the orthogonality between the two modes. The proposed antenna obtains a 100 MHz impedance bandwidth, determined by the reflection coefficient less than −10 dB. The measured gain of the sum pattern is 11.9 dBi at 10 GHz, while the null depth of the difference pattern is lower than −27 dB.

INDEX TERMS Monopulse antenna, substrate integrated waveguide (SIW), aperture efficiency, dual-mode resonant cavity.

I. INTRODUCTION

Monopulse antennas are commonly used for target-tracking in radar systems owe to their precision angle estimation capability. The conventional three-dimensional monopulse antennas, such as horn antennas, lens antennas and Cassegrain parabolic antennas, are bulky, costly and low integration which limits their practical application. Therefore, microstrip antenna arrays are applied in monopulse radars to achieve low profile and low cost [1]–[3]. However, the complex microstrip feeding network not only suffer serious transmission loss, but also cause spurious radiation especially in millimeter-wave band.

In order to reduce loss and spurious radiation, monopulse antennas using SIW technology have been investigated widely [4]–[8]. The SIW structure, a tradeoff between the metal waveguide and planar transmission line, is suitable for millimeter-wave applications because of its low loss, low cost and easy integration with planar circuit [9], [10]. A single dual V-type linearly tapered slot monopulse antenna (DVLTSA) is reported in [4]. The sum and difference beams are generated by utilizing the multimode SIW feeding technique. A Ka-band compact single layer SIW slots array antenna without any microstrip-like structures is designed for two-dimension monopulse application in [5]. A planar W-band SIW monopulse slot array antenna, with a 16-way divider, a sum-difference compactor and 16 × 16 slots integrated on a singlelayer printed circuit board (PCB), is proposed in [6]. In [7], a single-layer extremely thin dual circular-polarized monopulse feeder at W-Band, which is consist of a sequential rotated 2 × 2 tilted SIW slots antenna array and a SIW comparator, is realized for a prime focus reflector antenna. In addition, based on a novel magic-tee with a wide amplitude and phase balance bandwidth, 60 GHz 1-D and 2-D monopulse antenna arrays with 4 × 4 slots are designed in [8].

Although, the monopulse antennas or monopulse feeder in [4]–[8] are fabricated on a single layer PCB, the complex feeding network and monopulse comparator occupy a large area which causes a low aperture efficiency. Multilayer SIW

The associate editor coordinating the review of this manuscript and approving it for publication was Diego Masotti.

monopulse antennas, with a radiating slots array on the upper layer while the feeding network including the sum and difference comparator is placed on the lower bottom layer, can realize high aperture efficiency relatively [11]–[15]. However, multilayer SIW structure implementations often suffer from fabrication complexity and alignment problems. In [13], [14], the sum and difference beams were produced utilizing dual-mode hybrid cavities. This approach avoids the need of standard 3dB-coupler and 90-degree phase shifter which can simplify the design. However, it is a pity that these monopulse antennas are multi-layered and power divider is also needed. It is a big challenge to design a single-layer monopulse antenna based on SIW technology with compact structure and high aperture efficiency until now

High-gain and low-cost SIW slotted cavity antennas using high-order modes were presented in [16], [17]. The antennas have simple structure and high efficiency simultaneously, because no external feed network is need in their design. Using high-order mode slotted SIW cavity for radiation and two SIW cavities operating at different modes to realize the sum and difference beams is an effective method to improve the aperture efficiency of the monopulse antenna while keeping a compact single-layer structure. In our previous work [18], a single-layer SIW slots array monopulse antenna with aperture efficiency up to 21% is proposed. The sum beam is generated when one feeding cavity operating at TE_{410} mode, and the difference beam is generated when the other feeding cavity operating at TE_{310} mode. The feeding structure also occupies a large area, because two separate SIW feeding cavities are still required to implement the sum and difference beams and the feeding cavities are operating at the high-order modes Thus, further improvement in the aperture efficiency is limited.

In this communication, to improve the aperture efficiency further, the SIW slot array is excited by a single square SIW cavity operating at two degenerated modes (TE_{120} and TE_{210}), which have been used for dual- and circular- polarized applications widely [19], [20]. The high-order mode TE_{120} and TE_{210} in the square SIW feeding cavity are orthogonal. Thus, good isolation between the sum and difference ports is obtained. Comparing with the antenna proposed in [18], only one feeding cavity is needed and lower order modes are utilized to produce the sum and difference beams. Eventually, the aperture efficiency of the proposed antenna is improved up to 42%, while keeping a simple single-layer structure. To the best of our knowledge, the proposed antenna has the highest aperture efficiency among other published singlelayer monopulse antenna based an SIW technology.

The reminder of this communication is organized as follows. Section II describes the geometrical structure of the antenna and the mechanism of generating the sum and difference beams. Then, comparison between the simulated and measured results is given in Section III. In the end, conclusions are draw in Section III.

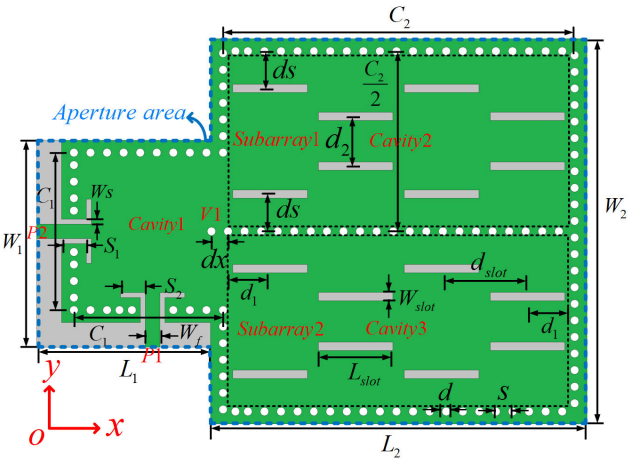

FIGURE 1. Geometry of the proposed monopulse antenna.

II. ANTENNA GEOMETRY AND OPERATING PRINCIPLE

A. ANTENNA GEOMETRY

The proposed monopulse antenna, as shown in Fig. 1, consists of two radiating cavities (cavities 2 and 3) and a dual-mode square cavity (cavity 1) with sum and difference ports (P_1 and P_2). There are two rows of 4×1 SIW-based longitudinal slots for radiation on the upper surface of cavities 2 and 3. The P_1 and P_2, a 50 Ω microstrip connected with a grounded coplanar waveguide (GCPW) feeding line, are used to excite the TE_{120} and TE_{210} modes in cavity 1, respectively. And the cavity 1 is coupled with cavities 2 and 3 through two open windows. The use of only one feeding cavity operating at high-order mode not only improves the antenna's aperture efficiency, but also reduces the structural complexity. Moreover, in order to make the sum and difference beams operate at the same frequency, a metallized via holes (V_1) with a diameter of 1 *mm* is placed near the right edge of cavity1 to slightly tune the resonant frequencies of the TE_{210} mode. The antenna is fabricated on a single-layer PCB (Rogers 4350B) with a relative permittivity of 3.48, a loss tangent of 0.0037 and a thickness of 0.762 *mm*. Optimized dimensional parameters are listed as follows: $L_1 = 21$ *mm*, $W_1 = 25$ *mm*, $L_2 = 45.5$ *mm*, $W_2 = 46.5$ *mm*, $C_1 = 19$ *mm*, $C_2 = 42.5$ *mm*, $d = 1$ *mm*, $s = 2$ *mm*, $dx = 2.0$ *mm*, $ds = 4.5$ *mm*, $S1 = S_2 = 3$ *mm*, $Ws = 0.6$ *mm*, $W_f = 1.75$ *mm*, $L_{slot} = 9$ *mm*, $W_{slot} = 1$ *mm*, $d_{slot} = 10.4$ *mm*, $d_1 = 5.2$ *mm*, $d_2 = 6$ *mm*.

B. OPERATING PRINCIPLE

The resonant modes of the cavity 1 along with the cavity 2 or 3, when they are separated and enclosed, are analyzed using the commercial software HFSS's eigenmode solver. Fig. 2 shows the electric field (E-field) magnitude distributions of the predicted two degenerated modes in the square dual-mode SIW cavity 1. The plus and minus signs indicate the orientation of the E-field. As can be observed,

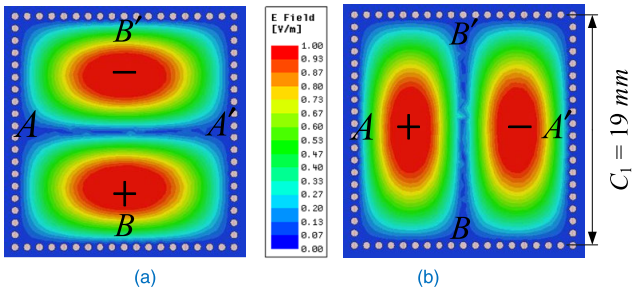

FIGURE 2. *E*-field distributions in the square dual-mode SIW cavity at 10 GHz: (a) the TE_{120} mode, (a) the TE_{210}mode.

the AA' and $BB'$are imaginary PEC boundary for the TE_{120} and TE_{210} modes, respectively. Therefore, only the TE_{120} mode will be excited when placing a feeding port along the sideBB' and only the TE_{210} mode will be obtained when placing a feeding port along the side AA'. Thus, good isolation between the two feeding ports along the sides AA' and BB' will be obtained due to the orthogonality between the two modes.

The *E*-field distribution of the operating resonant mode of cavity 2 or 3 is given in Fig. 3, in which there are 4×2 standing wave electric peak distribution inside the cavities 2 or 3 at equal distance, which means high-order mode TE_{420} mode has been successfully excited. Therefore, 4×2 SIW-based longitudinal slots can be etched on the upper surface of cavities 2 and 3 to form the subarrays (subarray 1 and 2) respectively. To radiate in phase, the slots of the subarray 1 or 2 should be positioned alternately on the opposite sides of the standing wave peak centerlines [16], [17].

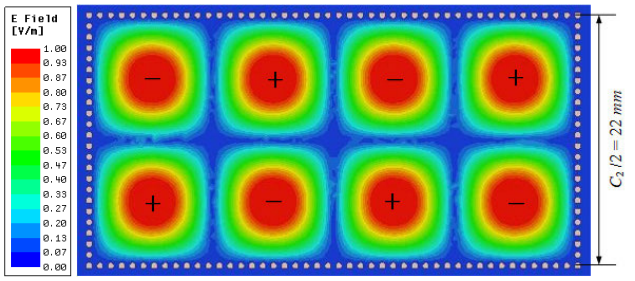

FIGURE 3. *E*-field distribution in the SIW cavity 2 or 3 operating at TE_{420} mode at 10 GHz.

The resonant frequency of the TE_{mn0} mode in the cavities 1, 2 and 3 can be obtained by the following formula

$$f_{TE_{mn0}} = \frac{c}{2\sqrt{\mu_r \varepsilon_r}} \sqrt{\left(\frac{m}{a}\right)^2 + \left(\frac{n}{b}\right)^2}, \quad (1)$$

where *c*is the speed of light in free space, μ_r and $\varepsilon_r$are the relative permeability and permittivity of the dielectric substrate respectively. And *m* and *n* represent the numbers of standing wave pattern along the *x*− and *y*− axes while *a* and *b* are the equivalent length of the SIW cavities along the corresponding axes. Therefore, the resonant frequencies of the TE_{120} and TE_{210} modes in the square SIW cavity 1 are the same.

The cavity 1 is coupled with cavities 2 and 3 through two open windows, and Fig. 4 presents the *E*-field magnitude distributions of the predicted two eigenmodes when the TE_{120} and TE_{210} modes are excited in cavity 1, respectively. As can be observed, the *E*-field in the region of the two open windows are almost null, thus the two open windows can be regarded as imaginary PEC boundary. Therefore, the TE_{120} and TE_{210} modes could be excited precisely, and the frequency of the two eigenmode in the composite structure is maintained at 10 GHz, because the composite structure can be regarded as three separated cavities.

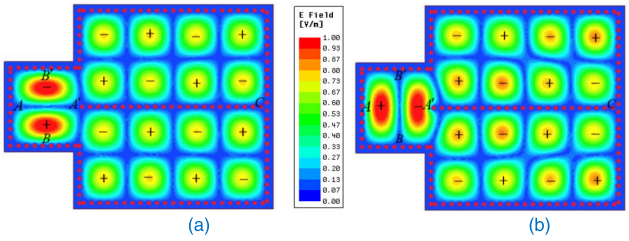

FIGURE 4. *E*-field distributions at 10 GHz: (a) the TE_{120} mode is excited in the cavity 1, (b) the TE_{210} mode is excited in the cavity 1.

As shown in Fig. 4, the *E*-filed distribution in cavities 2 and 3 is odd-symmetric about $A'C$ when the TE_{120} mode is excited in cavity 1, while it is even-symmetric when the TE_{210} mode is excited. This means that the *E*-filed distribution in cavities 2 and 3 is in-phase with same magnitude when placing a feeding port along the side BB' while it is out-of-phase when placing a feeding port along the side AA'. Therefore, the sum and difference beams will be obtained when the TE_{120} and TE_{210} modes are excited respectively. Furthermore, due to the strong *E*-field distribution for the TE_{210} mode and the weak even null *E*-field distribution for the TE_{120} mode near the region A', a metallized via hole near the region A' can slightly turn the resonant frequency of TE_{210} mode while keeping the TE_{120} mode's resonant frequency unchanged.

The standing wave electric distribution inside the cavities, as shown in Fig.4, leads us to etched 4×2 longitudinal radiating slots on the top surface of the cavities 2 and 3. The adjacent slots along the *x*-axis are spaced at half of a waveguide wavelength (d_{slot}), which will produce a 180° phase difference, and are positioned alternately on the opposite sides of the centerline of the standing-wave to add an additional 180° phase change. Therefore, the slots radiate in-phase.

III. SIMULATED AND MEASURED RESULTS

According to formula 1, the operating frequency of the antenna is mainly determined by the relative dielectric constant of the substrate and the dimension of the cavities, but the thickness of the substrate has little impact on it. Actually, a thicker substrate helps increase the bandwidth of the antenna. A higher relative dielectric constant helps in size reduction, but it decreases the bandwidth of the antenna and lower the gain of the antenna. In addition, the length of the

slots (L_{slot}) which is about half of a waveguide wavelength, and the position of the slots also affects the operating frequency as shown in Fig.5. As Fig.5 (a) and (b) show, the operating frequency will decrease when the slots are away from the central of the E-field standing wave, because the current distribution becomes stronger.

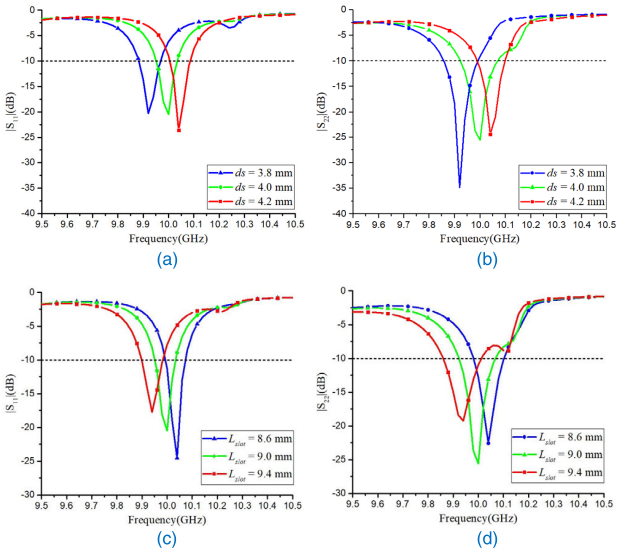

FIGURE 5. Simulated reflection coefficient varies with the slot position and the slot length: (a) and (c) the sum port $|S_{11}|$, (b) and (d) the difference port $|S_{22}|$.

Figure 6 shows the E-field magnitude distributions and vectors on the top surface of the proposed antenna operating at 10 GHz when the sum and difference ports (P_1 and P_2) are excited respectively. As can be observed in Fig.6 (c) and (d), the radiating E-field vectors of subarray 1 and 2 is in phase when port P_1 is excited and it is out of phase when port P_2 is excited. Thus, the sum and difference beam in E-plane could be generated, respectively. In addition, the energy coupled to the difference port P_2 is weak even null when the sum port P_1 is excited, and the same is true for the sum port P_1

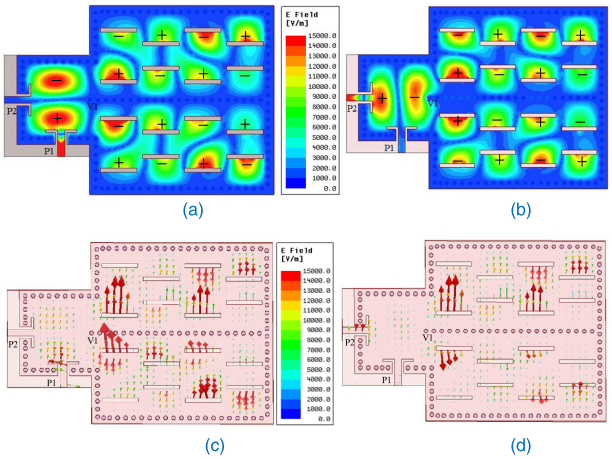

FIGURE 6. *E*-field magnitude distributions (top) and vectors (bottom) on the top surface of the antenna at 10 GHz: (a) and (c) when the sum port P_1 is excited, (b) and (d) when the difference port P_2 is excited.

when the difference port P_2 is excited as Fig. 6 (a) and (b) show. Therefore, the sum and difference ports (P_1 and P_2) has good isolation. Besides the need of good isolation, the operating frequencies of the sum and difference ports should be as consistent as possible. Moving the V_1 towards $-x$-axis will squeeze the E-field distribution of the TE_{210} mode in cavity 1 into a smaller room while the presence of V_1 has little influence on the TE_{120} mode's E-field distribution. As Fig. 7 shows, this will increase the operating frequency of the difference port while the sum port's operating frequency keeps unchanged. Moreover, the presence of V_1 may cause the difference beam a little asymmetry due to the machining error.

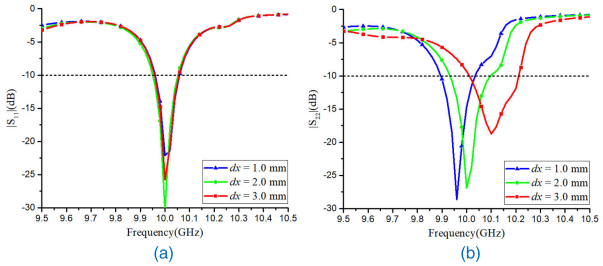

FIGURE 7. Simulated reflection coefficient when moving the V_1 towards $-x$-axis: (a) the sum port $|S_{11}|$, (b) the difference port $|S_{22}|$.

To validate the design, a prototype was fabricated and then measured. Fig. 8 shows the photograph of the fabricated prototype with two SMA connectors. The reflection coefficients of the antenna's sum and difference ports (S_{11} and S_{22}) including the transmission coefficient between them (S_{21}) were measured by a vector network analyzer (Agilent N9918A), and its radiation patterns were measured by an *NSI* far-field test system in a microwave chamber.

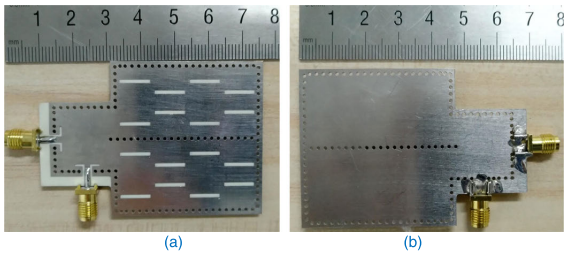

FIGURE 8. Photograph of the prototype antenna: (a) top view, (b) bottom view.

Figure 9 shows the simulated and measured S-parameters of the proposed antenna. The simulated impedance bandwidth of the sum port is about 100 MHz (determined by the reflection coefficient less than −10 dB) while the difference port's bandwidth is slightly wider. The predicted isolation between the sum and difference ports is better than 25 dB within the operating band. The measured results are in good agreement with the simulated except that the isolation is a little worse than the simulated. Due to the machining error, the E-field may be stronger than predicted in the region of the difference port P_2 when the sum ports P_1 is excited, and this will cause the maximum isolation point shift.

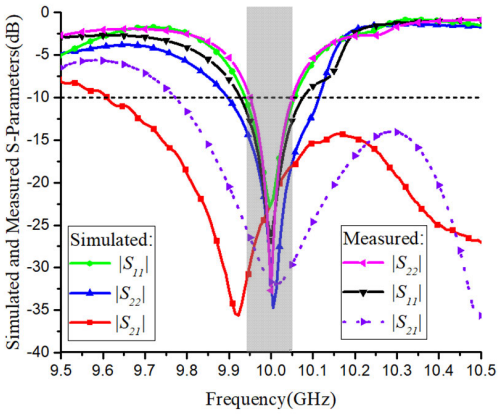

FIGURE 9. Simulated and measured S-parameters (S_{11}, S_{22} and S_{21}) of the proposed antenna.

The simulated and measured co- and cross- polarization radiation patterns of the sum and difference beams in the *yoz*-plane (E-plane) are given in Figs. 10 (a) and (b). And, Figs. 11 (a) and (b) show the simulated and measured co- and cross- polarization radiation patterns of the sum beam in the *xoz*-plane (H-plane). Because the radiation of the difference beam in the H-plane is nearly null, its radiation pattern is not given there. The simulated gain of the sum beam is 12.2 dBi in the normal direction while the null depth is lower than −36 dB. And the simulated gain of the difference beam is 8.9 and 9.4 dBi when the azimuth angle 'theta' is equal to −31° and 29°, respectively. The measured gain of the sum beam is 11.9 dBi and the null depth is about −27 dB. The measured gain of the difference beam is 9.1 and 9.3 dBi when the azimuth angle 'theta' is equal to −30° and 32°, respectively. Good agreement is obtained between the measured and simulated radiation patterns except the side lobe is higher than predicted slightly.

It is worth noting that the difference beam in the E-plane is a little asymmetric about *z*-axis (theta = 0°). This is because the presence of the sum port P_1 makes the antenna not symmetric around the *x*-axis perfectly which makes the excitation amplitude of subarray 1 and 2 is not entirely equal as Fig. 6(b) shows. Moving V_1 towards +y axis a little bit could make the excitation amplitude of subarray 1 and 2 as same as possible.

In traditional pulse compression monopulse radar, the precise distance of targets is obtained according to the time difference between the transmitted pulse signal and the target echo signal received in the sum channel and the angle information of targets is acquired by comparison of signals received in the sum and difference channels. Fig. 12 shows the simulated and measured gain difference between the sum and difference beams in the *xoz*-plane (E-plane). The simulated gain difference is lower than measured around the direction where the gain of the difference beam is minimum (Theta=0), because it's hard to measure the gain of the difference beam precisely due to the energy is too weak. The measured 3-dB beamwidth of the 'Sum-Difference' pattern is about 4° which is much less than that of the sum pattern. Thus, the monopulse working mechanism could improve the accuracy of angle

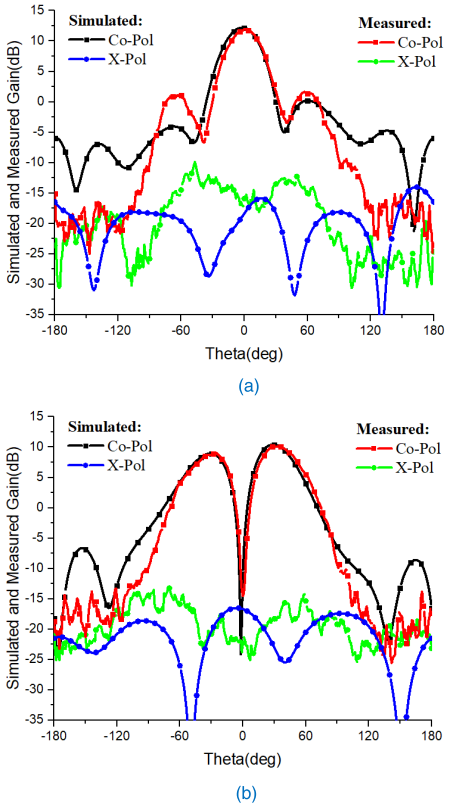

FIGURE 10. Simulated and measured co- and cross- polarization radiation patterns of the sum and difference beams in the *yoz*-plane: (a) the sum beam, (b) the difference beeam.

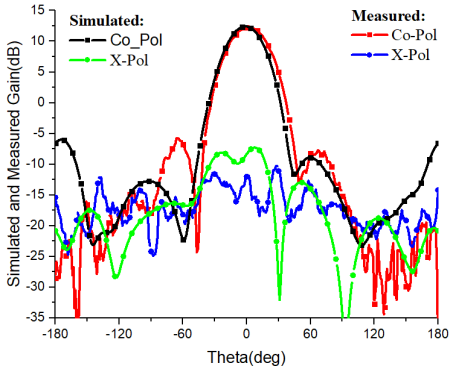

FIGURE 11. Simulated and measured co- and cross- polarization radiation patterns of the sum beam in the *xoz*-plane.

estimation without increasing the number of antenna elements.

The aperture efficiency of the proposed antenna is improved up to 42% determined by the following formula

$$\eta = \frac{\lambda^2 G}{4\pi A} \tag{2}$$

where λ is the wavelength in free space, *G* is the maximal gain of the antenna and *A* is area of the whole antenna's aperture which is enclosed by the blue dotted line in Fig. 1. The area of the antenna's aperture includes all substrate footprint area occupied by the radiation and feeding parts.

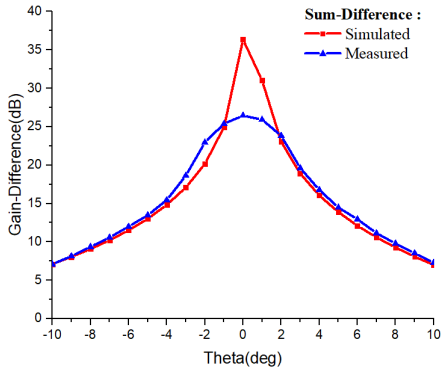

FIGURE 12. Simulated and measured gain difference between the sum and difference beams in the *xoz*-plane.

TABLE 1. Comparisons between the proposed antenna and previous works.

Ref.	FREQUENCY (GHz)	PCB layers	Aperture area (wavelength^2)	Gain (dBi)	Aperture efficiency
[5]	31.5	Single	150.6	18.7	3.9%
[6]	94.0	Single	1595.4	25.8	1.9%
[8] Type A	60.0	Single	37.1	15.3	7.3%
[8] Type B	60.0	Single	97.5	15.5	2.9%
[13]	9.9	Dual	1.6	12.3	82.4%
[14]	10.0	Dual	1.4	9.2	48.0%
[18]	5.8	Single	7.2	12.9	21.6%
This work	10.0	Single	2.9	11.9	42.0%

Because the gain of an antenna (G) is proportionate to S/λ^2, where S is the area of an antenna's radiation part. Thus, the aperture efficiency of an antenna is proportionate to S/A. Therefore, no matter what substrate is adopted and no matter what the operating frequency of an antenna is, the aperture efficiency of an antenna is only determined by the ratio of the radiation area of an antenna to the overall area of an antenna. Thus, with a similar gain, an antenna array with a simple feeding structure will have a higher aperture efficiency.

Comparisons between the proposed antenna and other previous SIW monopulse slots array antenna are presented in the Table 1. In [5] and [6], the feeding structures occupy a significantly large area of the antenna aperture which results in a low aperture efficiency. Relatively high aperture efficiency is achieved through dual-layer topology in [13] and [14]. However, multilayer SIW structure implementations often suffer from fabrication complexity and alignment problems especially in millimeter-wave band.

In our previous work [18], a single-layer SIW slots array monopulse antenna with aperture efficiency up to 21% is proposed by using high-order mode slotted SIW cavity for radiation and two separate SIW cavities operating at different modes to realize the sum and difference beams. The area occupied by the feeding and radiation parts are about 3.1 and 4.1 times the wavelength squared, respectively. The area of the feeding part is almost about three quarters that of the radiating part which limits further improvement in the aperture efficiency. In this work, the sum and difference beams are realized through a simple dual-mode feeding cavity rather than complex feeding structure. The area of the feeding and radiation parts is about 0.6 and 2.3 in the square of the wavelength, respectively. The area occupied by the feeding part is only about a quarter that of the radiating part, thus, a higher aperture efficiency is realized.

IV. CONCLUSION

In this communication, a single-layer planar integrated SIW slots array monopulse antenna operating at 10 GHz is proposed, fabricated and measured. A square dual-mode SIW resonant cavity is used to realize monopulse comparator which improves the antenna's aperture efficiency while keeping a planar single-layer structure. The sum and difference beams are obtained when the feeding cavity operates at two high-order modes (TE_{120} and TE_{210}), respectively. Owing to the orthogonality between the two modes, good isolation is achieved between the sum and difference ports.

Because of the needless of complex feeding network and the high-order dual-mode operating mechanism, the antenna's aperture efficiency is improved effectively. The area occupied by the feeding cavity is only about a quarter of that of the radiating cavity. It's worth mentioning that the antenna's aperture efficiency could be further improved when there are more slot radiation units. Good agreement is obtained between the simulated and measured results which proves the correctness of the design. The proposed monopulse antenna is a promising candidate for modern target-tracking systems due to its compact single-layer structure, low-loss, low-cost and easy integration with other planar circuits.

REFERENCES

[1] H. Wang, D.-G. Fang, and X. G. Chen, "A compact single layer monopulse microstrip antenna array," *IEEE Trans. Antennas Propag.*, vol. 54, no. 2, pp. 503–509, Feb. 2006.
[2] Z. W. Yu, G. M. Wang, and C. X. Zhang, "A broadband planar monopulse antenna array of C-band," *IEEE Antennas Wireless Propag. Lett.*, vol. 8, pp. 1325–1328, 2009.
[3] H. Kumar and G. Kumar, "Broadband monopulse microstrip antenna array for X-band monopulse tracking," *IET Microw., Antennas Propag.*, vol. 12, no. 13, pp. 2109–2114, Oct. 2018.
[4] Y. J. Cheng, W. Hong, and K. Wu, "Design of a monopulse antenna using a dual V-type linearly tapered slot antenna (DVLTSA)," *IEEE Trans. Antennas Propag.*, vol. 56, no. 9, pp. 2903–2909, Sep. 2008.
[5] B. Liu, W. Hong, Z. Kuai, X. Yin, G. Luo, J. Chen, H. Tang, and K. Wu, "Substrate integrated waveguide (SIW) monopulse slot antenna array," *IEEE Trans. Antennas Propag.*, vol. 57, no. 1, pp. 275–279, Jan. 2009.
[6] Y. J. Cheng, W. Hong, and K. Wu, "94 GHz substrate integrated monopulse antenna array," *IEEE Trans. Antennas Propag.*, vol. 60, no. 1, pp. 121–129, Jan. 2012.
[7] P. F. Kou and Y. J. Cheng, "A dual circular-polarized extremely thin monopulse feeder at W-band for prime focus reflector antenna," *IEEE Antennas Wireless Propag. Lett.*, vol. 18, no. 2, pp. 231–235, Feb. 2019.
[8] J. Zhu, S. Liao, S. Li, and Q. Xue, "60 GHz substrate-integrated Waveguide-based monopulse slot antenna arrays," *IEEE Trans. Antennas Propag.*, vol. 66, no. 9, pp. 4860–4865, Sep. 2018.

[9] C. Di Paola, K. Zhao, S. Zhang, and G. F. Pedersen, "SIW multibeam antenna array at 30 GHz for 5G mobile devices," *IEEE Access*, vol. 7, pp. 73157–73164, 2019.
[10] W. Li, X. Tang, and Y. Yang, "Design and implementation of SIW cavity-backed dual-polarization antenna array with dual high-order modes," *IEEE Trans. Antennas Propag.*, vol. 67, no. 7, pp. 4889–4894, Jul. 2019.
[11] K. Tekkouk, M. Ettorre, L. Le Coq, and R. Sauleau, "SIW pillbox antenna for monopulse radar applications," *IEEE Trans. Antennas Propag.*, vol. 63, no. 9, pp. 3918–3927, Sep. 2015.
[12] T. Li, W. Dou, and H. Meng, "A monopulse slot array antenna based on dual-layer substrate integrated waveguide (SIW)," in *Proc. IEEE 5th Asia–Pacific Conf. Antennas Propag. (APCAP)*, Kaohsiung, Taiwan, Jul. 2016, pp. 373–374.
[13] H. Gharibi and F. Hodjatkashani, "Design of a compact high-efficiency circularly polarized monopulse cavity-backed substrate integrated waveguide antenna," *IEEE Trans. Antennas Propag.*, vol. 63, no. 9, pp. 4250–4256, Sep. 2015.
[14] H. Gharibi and F. H. Kashani, "Design of a compact circularly polarized dual-mode monopulse cavity-backed substrate integrated waveguide antenna," *IEEE Antennas Wireless Propag. Lett.*, vol. 14, pp. 519–522, 2015.
[15] Y. Liu, H. Yang, Z. Jin, and J. Zhu, "Multi-beam monopulse substrate integrated waveguide slot array antenna," *IET Microw., Antennas Propag.*, vol. 13, no. 2, pp. 142–148, Feb. 2019.
[16] W. Han, F. Yang, R. Long, L. Zhou, and F. Yan, "Single-fed low-profile high-gain circularly polarized slotted cavity antenna using a high-order mode," *IEEE Antennas Wireless Propag. Lett.*, vol. 15, pp. 110–113, 2016.
[17] W. Han, F. Yang, J. Ouyang, and P. Yang, "Low-cost wideband and high-gain slotted cavity antenna using high-order modes for millimeter-wave application," *IEEE Trans. Antennas Propag.*, vol. 63, no. 11, pp. 4624–4631, Nov. 2015.
[18] F. Cao, D. Yang, J. Pan, D. Geng, and H. Xiao, "A compact single-layer substrate-integrated waveguide (SIW) monopulse slot antenna array," *IEEE Antenna Wireless Propag. Lett.*, vol. 16, pp. 2755–2758, 2017.
[19] G. Q. Luo, Z. F. Hu, Y. Liang, L. Y. Yu, and L. L. Sun, "Development of low profile cavity backed crossed slot antennas for planar integration," *IEEE Trans. Antennas Propag.*, vol. 57, no. 10, pp. 2972–2979, Oct. 2009.
[20] C. Hua, M. Liu, and Y. Lu, "Planar integrated substrate integrated waveguide circularly polarized filtering antenna," *Int. J. RF Microw. Comput. Aided Eng.*, vol. 29, no. 2, Feb. 2019, Art. no. e21517.

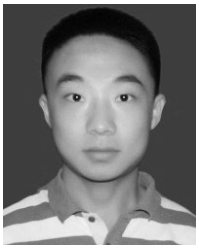

TIANMING YANG received the B.E. degree from the School of Electronic Engineering, University of Electronic Science and Technology of China, in 2016, where he is currently pursuing the Ph.D. degree. His research interest includes antenna design and theory.

ZHIQIN ZHAO (SM'05) received the B.S., M.S., and Ph.D. degrees in electronic engineering from the University of Electronic Science and Technology of China (UESTC), Chengdu, China, in 1990, 1993, and 1996, respectively, and the Ph.D. degree in electrical engineering from Oklahoma State University, Stillwater, OK, USA, in 2002. From 1996 to 1999, he was with the Department of Electronic Engineering, UESTC. From 2000 to 2002, he researched rough surface scattering as a Research Assistant with the School of Electrical and Computer Engineering, Oklahoma State University. From 2003 to 2006, he was a Postdoctoral Research Associate, later a Research Scientist, with the Department of Electrical and Computer Engineering, Duke University, Durham, NC, USA. In April 2006, he joined the School of Electronic Engineering, UESTC, as a Professor. He has authored or coauthored more than 200 refereed journal articles and conference articles and owned nine authorized patents. His current research interests include signal processing, electromagnetics and microwave engineering, remote sensing, and biomedical imaging. Dr. Zhao is a member of Phi Kappa Phi Honor Society.

DEQIANG YANG received the B.S., M.S., and Ph.D. degrees in electromagnetic field and microwave technique from the University of Electronic Science and Technology of China (UESTC), Chengdu, China, in 1992, 2006, and 2012, respectively, where he is currently a Professor. His research interests include antenna theories and techniques, antenna measurements, and the development of sensors for UWB systems.

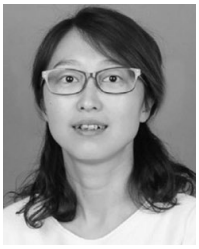

XIANFENG LIU received the B.S. and M.S. degrees in electromagnetic field and microwave technique from the University of Electronic Science and Technology of China, Chengdu, China, in 1998 and 2001, respectively, where she is currently a Lecturer. Her research interests include electromagnetic theories and computations, and antenna theories and designs.

QING-HUO LIU (S'88–M'89–SM'94–F'05) received the B.S. and M.S. degrees in physics from Xiamen University, Fujian, China, in 1983 and 1986, respectively, and the Ph.D. degree in electrical engineering from the University of Illinois at Urbana-Champaign, in 1989. He was with the Electromagnetics Laboratory, University of Illinois at Urbana-Champaign, as a Research Assistant, from September 1986 to December 1988, and as a Postdoctoral Research Associate, from January 1989 to February 1990. He was a Research Scientist and the Program Leader with Schlumberger-Doll Research, Ridgefield CT, from 1990 to 1995. From 1996 to May 1999, he was an Associate Professor with New Mexico State University, Albuquerque. Since June 1999, he was been with Duke University, Durham, NC, where he is currently a Professor of electrical and computer engineering. He is also a Visiting Professor with the University of Electronic Science and Technology of China (UESTC), Chengdu. He has published more than 350 articles in refereed journals and conference proceedings. His research interests include computational electromagnetics and acoustics, inverse problems, geophysical subsurface sensing, biomedical imaging, electronic packaging, and the simulation of photonic and nano devices. Dr. Liu is a member of Phi Kappa Phi, Tau Beta Pi, a Full Member of the U.S. National Committee of URSI Commissions B and F, and a Fellow of the Acoustical Society of America. He received the 1996 Presidential Early Career Award for Scientists and Engineers (PECASE) from the White House, the 1996 Early Career Research Award from the Environmental Protection Agency, and the 1997 CAREER Award from the National Science Foundation. Currently, he serves as an Associate Editor for *Radio Science*, and the IEEE TRANSACTIONS ON GEOSCIENCE AND REMOTE SENSING, which he also served as a Guest Editor for a Special Issue on Computational Methods.